Electron-Phonon Coupling from *Ab Initio* Linear-Response Theory within the *GW* Method: Correlation-Enhanced Interactions and Superconductivity in $\mathrm{Ba}_{1-x}\mathrm{K}_x\mathrm{BiO}_3$

Zhenglu Li, Gabriel Antonius, Meng Wu, Felipe H. da Jornada, and Steven G. Louie[*]
Department of Physics, University of California at Berkeley, California 94720, USA and Materials Sciences Division,
Lawrence Berkeley National Laboratory, Berkeley, California 94720, USA

(Received 18 July 2018; revised manuscript received 15 February 2019; published 10 May 2019)

We present a new first-principles linear-response theory of changes due to perturbations in the quasiparticle self-energy operator within the *GW* method. This approach, named *GW* perturbation theory (*GW*PT), is applied to calculate the electron-phonon (*e*-ph) interactions with the full inclusion of the *GW* nonlocal, energy-dependent self-energy effects, going beyond density-functional perturbation theory. Avoiding limitations of the frozen-phonon technique, *GW*PT gives access to *e*-ph matrix elements at the *GW* level for *all* phonons and scattering processes, and the computational cost scales *linearly* with the number of phonon modes (wave vectors and branches) investigated. We demonstrate the capabilities of *GW*PT by studying the *e*-ph coupling and superconductivity in $\mathrm{Ba}_{0.6}\mathrm{K}_{0.4}\mathrm{BiO}_3$. We show that many-electron correlations significantly enhance the *e*-ph interactions for states near the Fermi surface, and explain the observed high superconductivity transition temperature of $\mathrm{Ba}_{0.6}\mathrm{K}_{0.4}\mathrm{BiO}_3$ as well as its doping dependence.

DOI: 10.1103/PhysRevLett.122.186402

First-principles calculation of electron-phonon (*e*-ph) coupling [1] is of tremendous interest as it serves as a nonempirical approach to predict and understand a number of phenomena in condensed matter physics and materials physics, such as phonon-mediated superconductivity, electrical and thermal transport, quasiparticle energy renormalization, charge-density wave (CDW), and vibrational features in optical spectra. By formulating a linear-response theory of density functional theory (DFT) [2] to phonon perturbations, density-functional perturbation theory (DFPT) [3–6] has been the prevailing and most efficient *ab initio* method to study the *e*-ph interactions within DFT. The *e*-ph coupling treated in DFPT is only approximate since the DFT orbital eigenvalues are not the true electron (or quasiparticle) energies. This is reflected in that, in general, the Kohn-Sham eigenvalues do not yield accurate band gaps and band widths nor information on lifetimes [7,8]. The exchange-correlation potentials V_{xc} in DFT [such as those in the local-density approximation (LDA) [9] or the generalized gradient approximation (GGA) [10]] can only be at best considered as an approximation to the nonlocal, frequency-dependent self-energy operator Σ.

The *GW* approximation [7,8,11–13] has proven, for many materials, to be an accurate *ab initio* method in capturing the many-electron correlation effects in the evaluation of the quasiparticle energies. In the *GW* approximation, the self-energy operator Σ is expanded in terms of the single-particle Green's function G and the screened Coulomb interaction W to first order, i.e., $\Sigma = iGW$, hence named the *GW* method. By combining the frozen-phonon technique with *GW* calculations, previous studies [14–20] have found that many-electron *corrections* to DFT *e*-ph coupling strength are essential to accurately describe a number of phenomena, such as the phonon dispersion in graphene and graphite [14,15], the temperature-dependent band gap in diamond [18], and superconductivity in $\mathrm{Ba}_{0.6}\mathrm{K}_{0.4}\mathrm{BiO}_3$ [17]. However, the frozen-phonon technique is limited to only investigate couplings to phonon wave vectors that are commensurate to a large supercell, which makes it prohibitive to achieve a fine sampling of the Brillouin zone (BZ). More importantly, frozen-phonon calculations can only provide *some* intraband part of the *e*-ph matrix elements *indirectly* and an overall *e*-ph coupling strength by examining band energy shifts. The *e*-ph matrix elements between different bands and for wave vectors across the full BZ—the essential ingredient of microscopic *e*-ph formulations of many physical phenomena—are *not* available within frozen-phonon methods [1,17,19,20]. The importance of self-energy effects in *e*-ph coupling and the severe limitations of the frozen-phonon *GW* technique thus point to a strong necessity for a linear-response *GW* theory (similar in spirit as DFPT [3–6]) to efficiently and accurately calculate the quasiparticle *e*-ph interactions at the *GW* level [1,17,19,20].

In this Letter, for the first time, we present a first-principles linear-response *GW* method to external perturbations, which we call *GW* perturbation theory (*GW*PT). In this scheme, the first-order change of the self-energy operator to a phonon perturbation $\Delta_{\mathbf{q}\nu}\Sigma$ is constructed from a linear-response calculation, which is performed within a single primitive unit cell for any phonon wave vector $\mathbf{q}$ and phonon branch ν. This method avoids the use of supercells, and the computational cost naturally scales linearly with the number of phonon modes needed. More importantly, from a physics view point, it provides the e-ph matrix elements at the GW level for any pairs of electronic states directly and efficiently, making GWPT a desirable *ab initio* method to systematically study e-ph interactions including many-electron self-energy effects. We demonstrate the power of the GWPT method by studying the e-ph coupling and superconductivity in $\mathrm{Ba_{0.6}K_{0.4}BiO_3}$ [21–23] as well as other doping concentrations away from $x = 0.4$. We find that the GW self-energy renormalizes the DFT-LDA e-ph matrix elements *nonuniformly* across the BZ, and enhances the e-ph coupling constant λ by a factor of 2.4. The GWPT-calculated $\lambda = 1.14$ is strong enough to account for the high superconducting transition temperature T_c in $\mathrm{Ba_{0.6}K_{0.4}BiO_3}$. We show that the doping dependence in the superconductivity is mainly from a density of states (DOS) effect.

Here the GWPT method is formulated for phonon perturbations, but it can straightforwardly be generalized to other perturbations such as electric field and strain. We present the theory for crystals with time-reversal symmetry (TRS), and spin indices are omitted for simplicity. The key quantity is the e-ph coupling matrix element $g_{mn\nu}(\mathbf{k},\mathbf{q})$. The e-ph matrix element at the GW level can be constructed in a similar way that the quasiparticle energy is constructed [8], with the contribution from the GW self-energy replacing that from the exchange-correlation functional $V_{\mathrm{xc}}(\mathbf{r})$ in DFT; that is,

$$g^{GW}_{mn\nu}(\mathbf{k},\mathbf{q}) = g^{\mathrm{DFT}}_{mn\nu}(\mathbf{k},\mathbf{q}) - \langle\psi_{m\mathbf{k}+\mathbf{q}}|\Delta_{\mathbf{q}\nu}V_{\mathrm{xc}}|\psi_{n\mathbf{k}}\rangle + \langle\psi_{m\mathbf{k}+\mathbf{q}}|\Delta_{\mathbf{q}\nu}\Sigma|\psi_{n\mathbf{k}}\rangle, \tag{1}$$

where

$$g^{\mathrm{DFT}}_{mn\nu}(\mathbf{k},\mathbf{q}) = \langle\psi_{m\mathbf{k}+\mathbf{q}}|\Delta_{\mathbf{q}\nu}V^{\mathrm{KS}}|\psi_{n\mathbf{k}}\rangle \tag{2}$$

is the e-ph matrix element at the DFT level [1]. V^{KS} is the total Kohn-Sham potential in DFT, and $\psi_{n\mathbf{k}}$ and $\psi_{m\mathbf{k}+\mathbf{q}}$ are the wave functions of the initial and final electron states involved in the scattering process, with band indices n and m at wave vectors $\mathbf{k}$ and $\mathbf{k}+\mathbf{q}$, respectively. The differential perturbation operator $\Delta_{\mathbf{q}\nu}$ gives the linear change in the quantity it operates on, when the system is perturbed with a phonon mode labeled by $\mathbf{q}\nu$ with the atoms displaced by the zero-point displacement amplitude [1]. The dimensionless operator $\Delta_{\mathbf{q}\nu}$ carries a crystal momentum of $\mathbf{q}$, and is explicitly defined as

$$\Delta_{\mathbf{q}\nu} = \sqrt{\frac{\hbar}{2\omega_{\mathbf{q}\nu}}}\sum_{\kappa\alpha}\frac{1}{\sqrt{M_\kappa}}e_{\kappa\alpha,\nu}(\mathbf{q})\sum_{l}^{N_l}e^{i\mathbf{q}\cdot\mathbf{R}_l}\frac{\partial}{\partial\tau_{\kappa\alpha l}}, \tag{3}$$

where $\alpha = x, y, z$ labels the Cartesian directions, κ counts the atoms in the primitive unit cell, M_κ is the mass of the κth atom, $e_{\kappa\alpha,\nu}(\mathbf{q})$ is the $\kappa\alpha$ component of the νth eigenvector of the dynamical matrix at $\mathbf{q}$, $\omega_{\mathbf{q}\nu}$ is the phonon frequency, l labels the lth unit cell in the material, and $\mathbf{R}_l$ is the corresponding lattice position vector. In Eq. (3), the partial derivative is taken with respect to the atom coordinate $\tau_{\kappa\alpha l}$ of the κth atom, along the α direction, and in the lth unit cell. DFPT calculates $\Delta_{\mathbf{q}\nu}V^{\mathrm{KS}}$ by self-consistently solving the Sternheimer equation [1,6]. The Bloch wavefunction has the form $\psi_{n\mathbf{k}}(\mathbf{r}) = N_l^{-1/2}e^{i\mathbf{k}\cdot\mathbf{r}}u_{n\mathbf{k}}(\mathbf{r})$ where $u_{n\mathbf{k}}(\mathbf{r})$ is a lattice-periodic function. Therefore, the calculation of the e-ph matrix elements at either the DFPT or GWPT level is indeed done in a primitive unit cell, and no supercells are needed.

Now we construct the change in the self-energy operator. A change in Σ involves changes in G and W. Here, we use the constant-screening approximation [19] such that $\Delta_{\mathbf{q}\nu}W$ may be neglected compared to $\Delta_{\mathbf{q}\nu}G$ against small perturbations. The validity of this approximation has been verified by using frozen-phonon calculations in a previous study [19] and by our own calculations. It is expected to be generally valid in semiconductors where the charges are bounded in bonds, and in metals with large Fermi surfaces. With this approximation, the change in the self-energy operator in the frequency domain reads

$$\Delta_{\mathbf{q}\nu}\Sigma(\mathbf{r},\mathbf{r}';\varepsilon) = i\int\frac{d\varepsilon'}{2\pi}e^{-i\delta\varepsilon'}\Delta_{\mathbf{q}\nu}G(\mathbf{r},\mathbf{r}';\varepsilon-\varepsilon')W(\mathbf{r},\mathbf{r}';\varepsilon'), \tag{4}$$

where ε and ε' are energy variables, and $\delta = 0^+$. To construct $\Delta_{\mathbf{q}\nu}G$, we need the first-order change in the wave function [6],

$$\Delta_{\mathbf{q}\nu}\psi_{n\mathbf{k}}(\mathbf{r}) = \sum_m\frac{g^{\mathrm{DFT}}_{mn\nu}(\mathbf{k},\mathbf{q})}{\varepsilon_{n\mathbf{k}}-\varepsilon_{m\mathbf{k}+\mathbf{q}}}\psi_{m\mathbf{k}+\mathbf{q}}(\mathbf{r}), \tag{5}$$

where $\varepsilon_{n\mathbf{k}}$ and $\varepsilon_{m\mathbf{k}+\mathbf{q}}$ are the DFT eigenvalues. Using the knowledge that DFT eigenfunctions well approximate the quasiparticle wave functions of most materials [8], the change in the Green's function is written as

$$\Delta_{\mathbf{q}\nu}G(\mathbf{r},\mathbf{r}';\varepsilon) = \sum_{n\mathbf{k}}\frac{\Delta_{\mathbf{q}\nu}\psi_{n\mathbf{k}}(\mathbf{r})\psi^*_{n\mathbf{k}}(\mathbf{r}') + \psi_{n\mathbf{k}}(\mathbf{r})[\Delta_{-\mathbf{q}\nu}\psi_{n\mathbf{k}}(\mathbf{r}')]^*}{\varepsilon-\varepsilon_{n\mathbf{k}}-i\delta_{n\mathbf{k}}}, \tag{6}$$

where $\delta_{n\mathbf{k}} = 0^+$ for $\varepsilon_{n\mathbf{k}} < \varepsilon_F$ and $\delta_{n\mathbf{k}} = 0^-$ for $\varepsilon_{n\mathbf{k}} > \varepsilon_F$ at zero temperature, and ε_F is the Fermi energy. In Eq. (6), we have used $\Delta_{\mathbf{q}\nu}\varepsilon_{n\mathbf{k}} = 0$, which is true for $\forall\,\mathbf{q} \neq 0$ connecting nondegenerate states (see more discussions in the Supplemental Material [24]).

In our implementation of GWPT, a plane-wave basis is used. The matrix element of $\Delta_{\mathbf{q}\nu}\Sigma$ now becomes

$$
\begin{aligned}
&\langle \psi_{m\mathbf{k}+\mathbf{q}} | \Delta_{\mathbf{q}\nu} \Sigma(\mathbf{r}, \mathbf{r}'; \varepsilon) | \psi_{n\mathbf{k}} \rangle \\
&\quad = \frac{i}{2\pi} \sum_{n'} \sum_{\mathbf{p}\mathbf{G}\mathbf{G}'} \Big(\langle \psi_{m\mathbf{k}+\mathbf{q}} | e^{i(\mathbf{p}+\mathbf{G})\cdot\mathbf{r}} | \Delta_{\mathbf{q}\nu} \psi_{n'\mathbf{k}-\mathbf{p}} \rangle \langle \psi_{n'\mathbf{k}-\mathbf{p}} | e^{-i(\mathbf{p}+\mathbf{G}')\cdot\mathbf{r}'} | \psi_{n\mathbf{k}} \rangle \int d\varepsilon' \frac{W_{\mathbf{G}\mathbf{G}'}(\mathbf{p}, \varepsilon') e^{-i\delta\varepsilon'}}{\varepsilon - \varepsilon_{n'\mathbf{k}-\mathbf{p}} - i\delta_{n'\mathbf{k}-\mathbf{p}} - \varepsilon'} \\
&\qquad + \langle \psi_{m\mathbf{k}+\mathbf{q}} | e^{i(\mathbf{p}+\mathbf{G})\cdot\mathbf{r}} | \psi_{n'\mathbf{k}+\mathbf{q}-\mathbf{p}} \rangle \langle \Delta_{-\mathbf{q}\nu} \psi_{n'\mathbf{k}+\mathbf{q}-\mathbf{p}} | e^{-i(\mathbf{p}+\mathbf{G}')\cdot\mathbf{r}'} | \psi_{n\mathbf{k}} \rangle \int d\varepsilon' \frac{W_{\mathbf{G}\mathbf{G}'}(\mathbf{p}, \varepsilon') e^{-i\delta\varepsilon'}}{\varepsilon - \varepsilon_{n'\mathbf{k}+\mathbf{q}-\mathbf{p}} - i\delta_{n'\mathbf{k}+\mathbf{q}-\mathbf{p}} - \varepsilon'} \Big),
\end{aligned}
\tag{7}
$$

where $\mathbf{G}$ and $\mathbf{G}'$ are reciprocal lattice vectors, n' and $\mathbf{p}$ are the band index and wave vector for the internal summation, and $W_{\mathbf{G}\mathbf{G}'}(\mathbf{p}, \varepsilon')$ is the screened Coulomb interaction. In the construction of W, the full dielectric matrix within the random-phase approximation [33] is used. The Hybertsen-Louie generalized plasmon-pole model [8] is employed in this work for the energy convolution of ε', and we note that the extension to fully frequency-dependent sampling techniques [34] is straightforward. The energy dependence of $\Delta_{\mathbf{q}\nu}\Sigma(\varepsilon)$ is treated with the strategy that every matrix element is evaluated at both $\varepsilon_{n\mathbf{k}}$ and $\varepsilon_{m\mathbf{k}+\mathbf{q}}$, and the average value is taken [35]. Our calculation shows that the energy dependence of the matrix elements is small. Equation (7) completes Eq. (1) to get $g_{mn\nu}^{GW}(\mathbf{k}, \mathbf{q})$.

The above formalism of *GW*PT has been implemented in the BERKELEYGW code [34,36], and is interfaced with the ABINIT code [37] which provides the DFT and DFPT calculations that generate $\Delta_{\mathbf{q}\nu} V_{\mathrm{xc}}(\mathbf{r})$ and $\Delta_{\mathbf{q}\nu} \psi_{n\mathbf{k}}(\mathbf{r})$ (see Supplemental Material [24]). Spatial symmetries and TRS are used to reduce the phonon $\mathbf{q}$ grid [24]. The development of *GW*PT enables access to a lot of new physics where *e*-ph and many-electron interactions are strongly intertwined, especially in correlated materials. Accurate *e*-ph matrix elements and their distribution across BZ and bands calculated using *GW*PT are essential ingredients in the understanding of a number of important phenomena including superconductivity, electrical (thermal) transport, electron (phonon) lifetimes due to *e*-ph interactions, and temperature-dependent direct (indirect) optical absorptions.

We have applied our *GW*PT method (within a one-shot calculation, i.e., G_0W_0PT) to study superconductivity in $\mathrm{Ba_{0.6}K_{0.4}BiO_3}$ in its cubic perovskite phase [Fig. 1(a)], which has an experimentally measured superconducting T_c of 30–32K [21–23]. Previous *ab initio* studies [17,38] show that the *e*-ph coupling calculated within DFT-LDA is too weak to account for such a high T_c in this material, and frozen-phonon *GW* calculations indicate that many-electron self-energy effects may enhance *e*-ph interactions. However, the latter was estimated from a limited study of only a single $\mathbf{q}$-point calculation for one electronic state [17].

We first perform standard DFT and DFPT calculations on $\mathrm{Ba_{0.6}K_{0.4}BiO_3}$ using the GGA functional [10]. The calculated Fermi surface shows a regular rounded cubic shape [Fig. 1(b)] and is strongly nested. We verify our *GW*PT method by comparing its results against reference frozen-phonon *GW* results at a selected high symmetry $\mathbf{q}$ vector. We focus on the single band [labeled as n_0 and

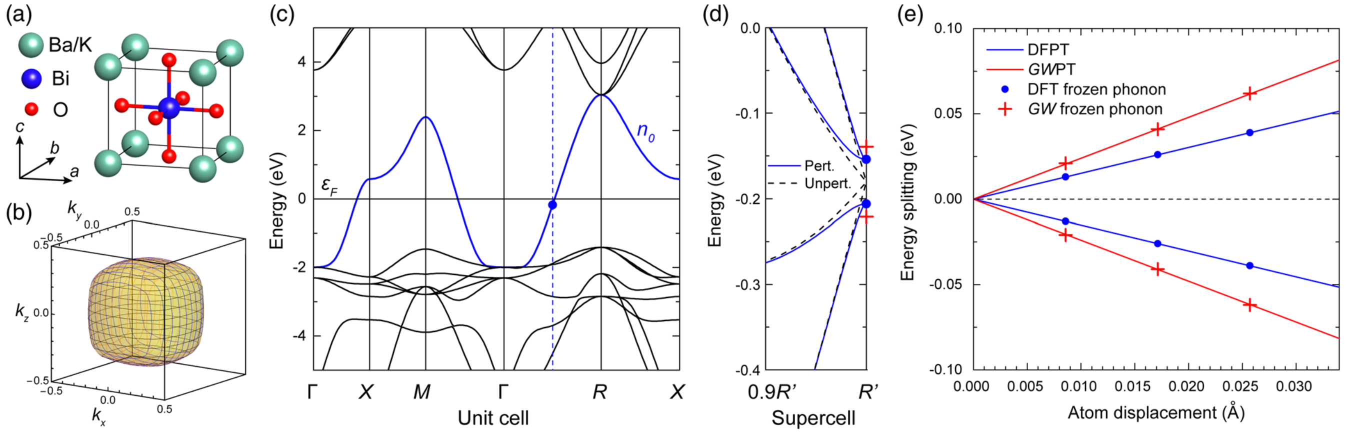

FIG. 1. (a) Crystal structure of $\mathrm{Ba_{0.6}K_{0.4}BiO_3}$ in the cubic perovskite phase. (b) Calculated Fermi surface of $\mathrm{Ba_{0.6}K_{0.4}BiO_3}$. (c) The DFT-GGA band structure of $\mathrm{Ba_{0.6}K_{0.4}BiO_3}$. The band of interest which crosses the ε_F (set to zero) is highlighted with blue color and labeled as n_0. The state at $\mathbf{k} = R/2$ (blue dashed line) indicated by the blue dot has a band energy slightly below ε_F. (d) The DFT band structure of a $2 \times 2 \times 2$ supercell. The R' point corresponds to the $\mathbf{k} = R/2$ point at the blue dashed line in (c). The degenerate level indicated by the blue dot in (c) splits upon the oxygen-atom-displacement perturbation (see Supplemental Material [24]) of 0.0171 Å. The corresponding *GW* quasiparticle energies are indicated by the red crosses. (e) Comparison of energy splitting-versus-displacement curves between perturbation theory and direct frozen-phonon (finite-difference) calculations.

highlighted in Fig. 1(c)] crossing ε_F, which is expected to give the dominant contribution to superconductivity. We are interested in $\mathbf{q} = R$, corresponding to a $2 \times 2 \times 2$ supercell with atom displacements (see details of the frozen-phonon calculation and more verifications in the Supplemental Material [24]). In the frozen-phonon calculation, the energy of the degenerate states at the BZ boundary [R' point in Fig. 1(d)] splits linearly with increasing displacement (when it is small enough). The slope in the change in energy with respect to displacement is given by a specific single e-ph matrix element that can be fitted from finite-difference frozen-phonon calculations, or *directly* calculated with the linear-response perturbation theory in a primitive unit cell. This type of e-ph matrix elements that connect degenerate states is the only one that frozen-phonon *GW* can relatively accurately calculate by making supercells [17], but *GW*PT can access *all* inter- and intraband e-ph matrix elements across the whole BZ with equal and high accuracy. As shown in Fig. 1(e), we find excellent agreement for this matrix element between frozen-phonon DFT and DFPT, and between frozen-phonon *GW* and *GW*PT, nicely verifying our *GW*PT method. Moreover, the DFPT and *GW*PT results are significantly different, illustrating the importance of the quasiparticle self-energy.

To study superconductivity in $\mathrm{Ba_{0.6}K_{0.4}BiO_3}$, we calculate the e-ph matrix elements that scatter quasiparticle states within the n_0 band by performing both DFPT and *GW*PT calculations on an $8 \times 8 \times 8$ **k** grid (full grid) and **q** grid (35 irreducible **q** points) [24]. These electronic states are coupled most strongly by phonons in the highest three optical branches [17,38]. As an illustration, we pick out one high-frequency oxygen stretching and breathing optical branch (labeled as ν_0 [24]), and plot the distribution of the strength of the e-ph matrix element $|g_{n_0 n_0 \nu_0}(\mathbf{k}, \mathbf{q})|$ varying **k** across the BZ for selected **q** points. Figures 2(a)–2(c) show the scatterings for $\mathbf{q} = R$ that are mostly relevant to superconductivity in this material. For this important phonon mode, *GW*PT almost uniformly enhances the value of the e-ph matrix elements g as compared to DFPT with an enhancement factor of ~1.6. This is because the character of the states on the Fermi surface of $\mathrm{Ba_{0.6}K_{0.4}BiO_3}$ is highly isotropic [39]. However, Figs. 2(d)–2(f) (and Fig. S3 [24]) show strong variances in the distribution of the e-ph matrix elements and also in the enhancement factor of *GW*PT over DFPT, due to the wave function character changing near the Γ point of either the initial or final states. These results, for the first time, systematically reveal the complex nature of many-electron renormalization of the e-ph interactions, demonstrating the capability and power of *GW*PT.

We evaluate the superconducting T_c of $\mathrm{Ba_{0.6}K_{0.4}BiO_3}$ using the McMillan-Allen-Dynes formula [40,41]. The e-ph coupling constant λ and the characteristic logarithmic-averaged phonon frequency $\omega_{\log}$ [1,40,41] are calculated using the e-ph matrix elements that scatter states within the n_0 band for all phonon modes, at both the DFPT and *GW*PT level (Table I). The correlation-enhanced e-ph coupling constant is directly reflected in the Eliashberg function $\alpha^2 F(\omega)$ by comparing the results from DFPT and *GW*PT in Fig. 3(a). The effective Coulomb parameter μ^* [1,40,41] is set to a reasonable physical range in Table I. DFPT severely underestimates the superconducting transition temperature, with the calculated T_c in the range of 0.61–6.1 K for μ^* in the range of 0.18–0.08. However, *GW*PT significantly increases T_c to the range of

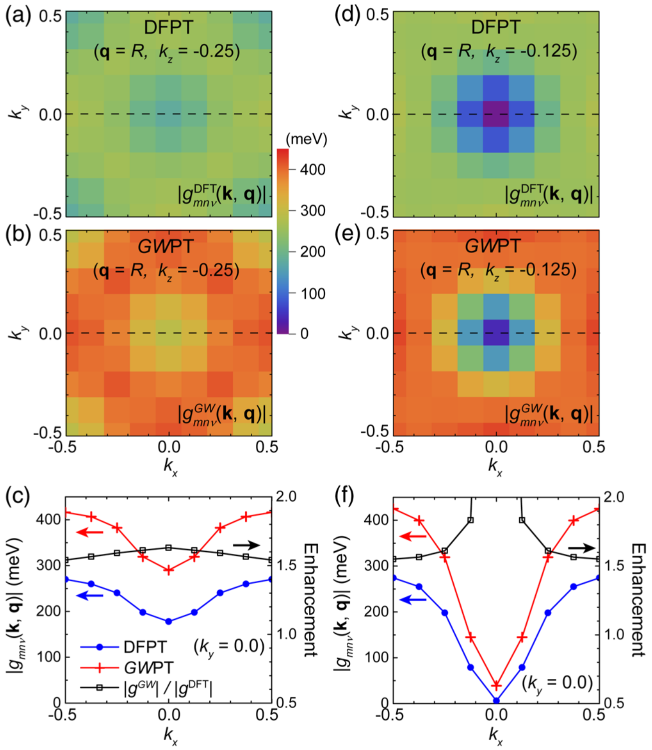

FIG. 2. Distribution of the absolute value of e-ph matrix elements $|g_{n_0 n_0 \nu_0}(\mathbf{k}, \mathbf{q} = R)|$ at (a) the DFPT and (b) *GW*PT level for $\mathrm{Ba_{0.6}K_{0.4}BiO_3}$, across the $k_x - k_y$ plane at fixed $k_z = -0.25$ of the BZ (reduced coordinates). Calculations are performed on the $8 \times 8 \times 8$ **k** grid for each **q** point. (c) Line profile of (a),(b) with $k_y = 0.0$, and the path is indicated by the dashed line in (a),(b). The enhancement factor of $|g^{GW}|/|g^{\mathrm{DFT}}|$ is also plotted. (d)–(f) Similar to (a)–(c), but with $\mathbf{q} = R$ in the $k_z = -0.125$ plane.

TABLE I. Calculated e-ph coupling constant λ, logarithmic-averaged phonon frequency $\omega_{\log}$, and superconducting transition temperature T_c (using the McMillan-Allen-Dynes formula) of $\mathrm{Ba_{0.6}K_{0.4}BiO_3}$. The effective Coulomb potential parameter μ^* is set to a reasonable physical range, giving the corresponding range of T_c. The experimentally measured T_c is 30–32 K [21,22].

	λ	$\omega_{\log}$ (K)	μ^*	T_c (K)
DFPT	0.47	488.2	0.18–0.08	0.61–6.1
*GW*PT	1.14	491.3	0.18–0.08	28.5–44.8

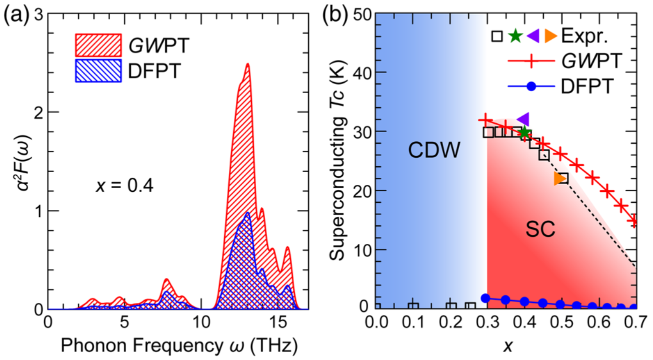

FIG. 3. (a) Eliashberg function $\alpha^2F(\omega)$ calculated for $Ba_{0.6}K_{0.4}BiO_3$ (i.e., $x = 0.4$) with *e*-ph matrix elements from *GW*PT and DFPT. (b) Phase diagram of $Ba_{1-x}K_xBiO_3$. Superconducting T_c (red crosses for *GW*PT and blue dots for DFTP) is calculated with $\mu^* = 0.16$. Experimental data are plotted as squares [23], star [21], left-pointing triangle [22], and right-pointing triangle [39]. Black dashed line represents the extrapolation of experimental data into doping range of $x > 0.5$, which is hard to access experimentally. From the superconducting (SC) phase towards undoped parent composition, for $x < 0.3$, the system undergoes a structural phase transition into the non-superconducting CDW phase.

28.5–44.8 K for the same range of μ^* (Table I), in good agreement with the experimentally measured T_c of 30–32 K [21–23]. These results highlight the importance of many-electron correlation effects in *e*-ph interactions [17] that are well captured by the *GW*PT method.

We further study the doping dependence of the superconductivity in $Ba_{1-x}K_xBiO_3$ (superconductivity is observed experimentally for $x > 0.3$) from first principles, calculated using a rigid-band approximation [24]. Figure 3(b) shows that the superconducting transition temperatures from *GW*PT nicely reproduce the size and shape of the superconducting half dome (however, results from DFPT fail significantly) in the phase diagram observed experimentally [21–23]. At doping concentration smaller than $x = 0.3$, the material is in an *insulating* CDW phase with strong structural distortions induced by phonon instability and the nested Fermi surface [17,23,38,42–44]. After $x = 0.4$, an increase in hole doping concentration x suppresses T_c, which is mainly due to a reduced DOS with a shrinking Fermi surface. With a reduced Fermi surface, the number of *e*-ph scattering channels decreases, weakening superconductivity (see Supplemental Material [24] for more analysis). Our *GW*PT results, along with the recent direct experimental observation of isotropic *s*-wave superconducting gap [39], strongly support that superconductivity in $Ba_{1-x}K_xBiO_3$ originates from unusually large *e*-ph interactions, due to many-electron effects.

In summary, we present the theoretical formulation, practical implementation, and application to $Ba_{1-x}K_xBiO_3$ of the newly developed *GW*PT method. *GW*PT is shown to be able to systematically and accurately investigate the rich *e*-ph physics at the *GW* level, beyond the accessibility of any other existing *ab initio* methods. The capability of *GW*PT demonstrates its great application potential to the study of the rich *e*-ph physics in a wide range of materials, going beyond DFT.

This work was supported by the Center for Computational Study of Excited-State Phenomena in Energy Materials (C2SEPEM) funded by the U.S. Department of Energy, Office of Basic Energy Sciences under Contract No. DE-AC02-05CH11231 at the Lawrence Berkeley National Laboratory, as part of the Computational Materials Sciences Program, which provided for theory development, code implementation, and calculations, and by the National Science Foundation under Grant No. DMR-1508412, which provided for benchmark studies and tests. Computational resources were provided by the National Energy Research Scientific Computing Center (NERSC), which is supported by the Office of Science of the U.S. Department of Energy under Contract No. DE-AC02-05CH11231, and the Extreme Science and Engineering Discovery Environment (XSEDE), which is supported by National Science Foundation under Grant No. ACI-1053575. The authors thank Y.-H. Chan, T. Cao, C. S. Ong, and H. J. Choi for helpful discussions.

---

[*] sglouie@berkeley.edu

[1] F. Giustino, Rev. Mod. Phys. **89**, 015003 (2017).
[2] R. O. Jones and O. Gunnarsson, Rev. Mod. Phys. **61**, 689 (1989).
[3] S. Baroni, P. Giannozzi, and A. Testa, Phys. Rev. Lett. **58**, 1861 (1987).
[4] X. Gonze, D. C. Allan, and M. P. Teter, Phys. Rev. Lett. **68**, 3603 (1992).
[5] S. Y. Savrasov, Phys. Rev. Lett. **69**, 2819 (1992).
[6] S. Baroni, S. De Gironcoli, A. Dal Corso, and P. Giannozzi, Rev. Mod. Phys. **73**, 515 (2001).
[7] M. S. Hybertsen and S. G. Louie, Phys. Rev. Lett. **55**, 1418 (1985).
[8] M. S. Hybertsen and S. G. Louie, Phys. Rev. B **34**, 5390 (1986).
[9] J. P. Perdew and A. Zunger, Phys. Rev. B **23**, 5048 (1981).
[10] J. P. Perdew, K. Burke, and M. Ernzerhof, Phys. Rev. Lett. **77**, 3865 (1996).
[11] L. Hedin, Phys. Rev. **139**, A796 (1965).
[12] L. Hedin and S. Lundqvist, Solid State Phys. **23**, 1 (1970).
[13] G. Onida, L. Reining, and A. Rubio, Rev. Mod. Phys. **74**, 601 (2002).
[14] M. Lazzeri, C. Attaccalite, L. Wirtz, and F. Mauri, Phys. Rev. B **78**, 081406(R) (2008).
[15] A. Grüneis, J. Serrano, A. Bosak, M. Lazzeri, S. L. Molodtsov, L. Wirtz, C. Attaccalite, M. Krisch, A. Rubio, F. Mauri, and T. Pichler, Phys. Rev. B **80**, 085423 (2009).
[16] C. Faber, J. L. Janssen, M. Côté, E. Runge, and X. Blase, Phys. Rev. B **84**, 155104 (2011).
[17] Z. P. Yin, A. Kutepov, and G. Kotliar, Phys. Rev. X **3**, 021011 (2013).

[18] G. Antonius, S. Poncé, P. Boulanger, M. Côté, and X. Gonze, Phys. Rev. Lett. **112**, 215501 (2014).

[19] C. Faber, P. Boulanger, C. Attaccalite, E. Cannuccia, I. Duchemin, T. Deutsch, and X. Blase, Phys. Rev. B **91**, 155109 (2015).

[20] B. Monserrat, Phys. Rev. B **93**, 100301(R) (2016).

[21] R. Cava, B. Batlogg, J. Krajewski, R. Farrow, L. Rupp Jr, A. White, K. Short, W. Peck, and T. Kometani, Nature (London) **332**, 814 (1988).

[22] P. Kumar, D. Hall, and R. G. Goodrich, Phys. Rev. Lett. **82**, 4532 (1999).

[23] S. Pei, J. D. Jorgensen, B. Dabrowski, D. G. Hinks, D. R. Richards, A. W. Mitchell, J. M. Newsam, S. K. Sinha, D. Vaknin, and A. J. Jacobson, Phys. Rev. B **41**, 4126 (1990).

[24] See Supplemental Material at http://link.aps.org/supplemental/10.1103/PhysRevLett.122.186402 for computational details, verification example of diamond, phonon spectrum calculations, more data on distribution of *e*-ph matrix elements in BZ, and further doping-dependence analysis, which includes Refs. [25–32].

[25] S. Poncé, Y. Gillet, J. Laflamme Janssen, A. Marini, M. Verstraete, and X. Gonze, J. Chem. Phys. **143**, 102813 (2015).

[26] D. R. Hamann, Phys. Rev. B **88**, 085117 (2013).

[27] M. van Setten, M. Giantomassi, E. Bousquet, M. Verstraete, D. Hamann, X. Gonze, and G.-M. Rignanese, Comput. Phys. Commun. **226**, 39 (2018).

[28] F. Giustino, M. L. Cohen, and S. G. Louie, Phys. Rev. B **76**, 165108 (2007).

[29] O. Hellman, I. A. Abrikosov, and S. I. Simak, Phys. Rev. B **84**, 180301(R) (2011).

[30] G. Kresse and J. Hafner, Phys. Rev. B **47**, 558 (1993).

[31] G. Kresse and D. Joubert, Phys. Rev. B **59**, 1758 (1999).

[32] T. Tadano, Y. Gohda, and S. Tsuneyuki, J. Phys. Condens. Matter **26**, 225402 (2014).

[33] M. S. Hybertsen and S. G. Louie, Phys. Rev. B **35**, 5585 (1987).

[34] J. Deslippe, G. Samsonidze, D. A. Strubbe, M. Jain, M. L. Cohen, and S. G. Louie, Comput. Phys. Commun. **183**, 1269 (2012).

[35] M. van Schilfgaarde, T. Kotani, and S. Faleev, Phys. Rev. Lett. **96**, 226402 (2006).

[36] Z. Li, G. Antonius, M. Wu, F. H. da Jornada, and S. G. Louie (to be published).

[37] X. Gonze, B. Amadon, P.-M. Anglade, J.-M. Beuken, F. Bottin, P. Boulanger, F. Bruneval, D. Caliste, R. Caracas, M. Côté *et al.*, Comput. Phys. Commun. **180**, 2582 (2009).

[38] V. Meregalli and S. Y. Savrasov, Phys. Rev. B **57**, 14453 (1998).

[39] C. H. P. Wen, H. C. Xu, Q. Yao, R. Peng, X. H. Niu, Q. Y. Chen, Z. T. Liu, D. W. Shen, Q. Song, X. Lou *et al.*, Phys. Rev. Lett. **121**, 117002 (2018).

[40] W. McMillan, Phys. Rev. **167**, 331 (1968).

[41] P. B. Allen and R. Dynes, Phys. Rev. B **12**, 905 (1975).

[42] M. Braden, W. Reichardt, W. Schmidbauer, A. Ivanov, and A. Y. Rumiantsev, J. Supercond. **8**, 595 (1995).

[43] N. C. Plumb, D. J. Gawryluk, Y. Wang, Z. Ristić, J. Park, B. Q. Lv, Z. Wang, C. E. Matt, N. Xu, T. Shang *et al.*, Phys. Rev. Lett. **117**, 037002 (2016).

[44] A. Khazraie, K. Foyevtsova, I. Elfimov, and G. A. Sawatzky, Phys. Rev. B **98**, 205104 (2018).